RNA-templated fluorescent Zn/PbS (PbS + Zn2+) supernanostructures

ARTICLE *in* THE JOURNAL OF PHYSICAL CHEMISTRY C · MAY 2009

Impact Factor: 4.77 · DOI: 10.1021/jp811402h

2 AUTHORS:

Anil Kumar
Indian Institute of Technology Roorkee
87 PUBLICATIONS **1,021** CITATIONS
SEE PROFILE

Anshuman Jakhmola
University of Kentucky
11 PUBLICATIONS **165** CITATIONS
SEE PROFILE

RNA-Templated Fluorescent Zn/PbS (PbS + Zn^{2+}) Supernanostructures

Anil Kumar*,†,‡ and Anshuman Jakhmola†

Department of Chemistry and Centre of Nanotechnology, Indian Institute of Technology Roorkee, Roorkee 247667, India

Received: December 26, 2008; Revised Manuscript Received: April 7, 2009

Synthesis of novel Zn/PbS (Zn^{2+} + PbS) fluorescent nanostructures of varied morphology and dimension has been reported. Zn^{2+} passivates the surface of RNA-templated PbS by binding to the specific sites of RNA through PO_2^- and purine bases and controls the dynamics of charge carriers, electronic properties, and growth of PbS in the nanocomposite. For a typical molar ratio of Pb/S = 2, the addition of 2×10^{-3} mol dm^{-3} of excess Zn^{2+} results in one-dimensional growth of spherical particles of RNA-mediated PbS to form nanofibers via several metastable self-assembled supernanostructures. The addition of Zn^{2+} enhances the fluorescence intensity of the 680 nm band. The nanofibers produced upon aging display a strong narrow emission band (fwhm $\leq$80 nm) at 680 nm having a quantum efficiency of 12 $\pm$ 0.2%. An increase in the fluorescence quantum efficiency with increasing Zn^{2+} is also evidenced by a drastic increase in fluorescence lifetime from 0.06 μs in its absence to 0.23 μs for the colloids containing 2×10^{-3} mol dm^{-3} Zn^{2+}, which is further increased to 0.27 μs upon aging. These studies demonstrate a correlation between the morphology of nanostructures and their electronic properties.

Introduction

A systematic organization of colloidal semiconductor nanoparticles in different shapes and dimensions has attracted a large attention due to their potential applications in making nanoelectronic, photonic, and optical devices.[1−6] The formation of different nanostructures and nanocomposites in nature through self-organization of biological molecules and inorganic materials has generated great interest in the utilization of the three-dimensional network of biological molecules for the synthesis of tailored nanostructures with desired properties.[7,8] The generation of self-assemblies from nanoparticles with a precise control of its chemical composition is a challenging task in order to fabricate nanoscale devices using these molecules. Lately, the functionalities of different biopolymers, specifically proteins,[9] nucleotides,[10,11] DNA,[2,12,13] and RNA[14−16] have been exploited as templates for their fabrication. In the recent past, nanostructures of PbS have been widely studied because of its extensive applications in photoluminescent devices,[17] solar cells,[18,19] telecommunications[20] and biological labeling.[21,22]

In the present study for the first time we report the synthesis and characterization of crystalline Zn^{2+} passivated quantized (Q)-PbS (Zn/PbS) novel nanostructures using optical, emission, field emission scanning electron microscopy (FE-SEM) coupled with energy dispersive X-ray (EDX), transmission electron microscopy (TEM), and IR and NMR spectroscopy. Interestingly, it demonstrated a transformation in their morphology from quantum dots to nanofibers via formation of nanowires under varied experimental conditions and produces efficient visible light-emitting PbS grown on RNA template. Growth of the self-assembly has been monitored by aging of colloids over a period of two and one-half months. Charge dynamics in these systems has been analyzed by single photon counter techniques.

* Corresponding author: anilkfcy@iitr.ernet.in; fax, +91-1332-273560; phone, +91-1332-285799.
† Department of Chemistry.
‡ Centre of Nanotechnology.

Results and Discussion

The experimental conditions for the synthesis of zinc-passivated RNA-capped Q-PbS were optimized by monitoring its optical and emission behavior as a function of [Zn^{2+}] for different molar ratios of Pb/S (1 to 3). The best electronic features were observed for PbS having a Pb/S molar ratio of 2. The initial addition of Zn^{2+} between 1×10^{-4} and 5×10^{-4} mol dm^{-3} in various increments to RNA-capped Q-PbS did not influence the optical absorption due to these particles appreciably. A further increase in [Zn^{2+}] up to 2×10^{-3} mol dm^{-3}, however, causes a slight increase in absorption in the visible region accompanied with a small decrease in absorption in the UV region, depicting an isosbestic point at 602 nm (2.05 eV). The fluorescence of these colloids is though enhanced in the entire concentration range of Zn^{2+}. For the addition of 2×10^{-3} mol dm^{-3} Zn^{2+} the fluorescence intensity is increased by a factor of more than 7.5 and blue-shifted the fluorescence maximum to higher energy from 675 nm (1.83 eV) to 669 nm (1.85 eV) compared to those observed in the absence of Zn^{2+} (Figure S1 in Supporting Information). A further addition of zinc made this solution turbid. An increase in pH of Zn/PbS nanocomposites from 9.8 to 11.2, keeping [RNA], [Pb^{2+}], and [Zn^{2+}] constant, did not exhibit any appreciable change in the absorption characteristics but resulted in a decrease in the fluorescence intensity (~35%) of these particles unlike RNA-mediated Q-PbS, where an increase in pH resulted in the loss of its excitonic features associated with a decrease in the fluorescence intensity of similar magnitude. Synthesis of these colloids at higher temperature (>80 °C) results in the production of a nonfluorescing dull brown solution having structureless absorption at the onset of absorption and extending into the near-IR region. It thus depicted the characteristics of an indirect band gap semiconductor. At high pH RNA may hydrolyze slowly to yield shorter fragments and eventually a mixture of 2′ and 3′ nucleoside monophosphates, whereas at high temperature RNA is denatured.[23] A reversal in the order of addition of Pb^{2+} and Zn^{2+}, i.e., when Zn^{2+} was added to RNA solution prior to Pb^{2+}

10.1021/jp811402h CCC: $40.75
Published on Web 05/11/2009

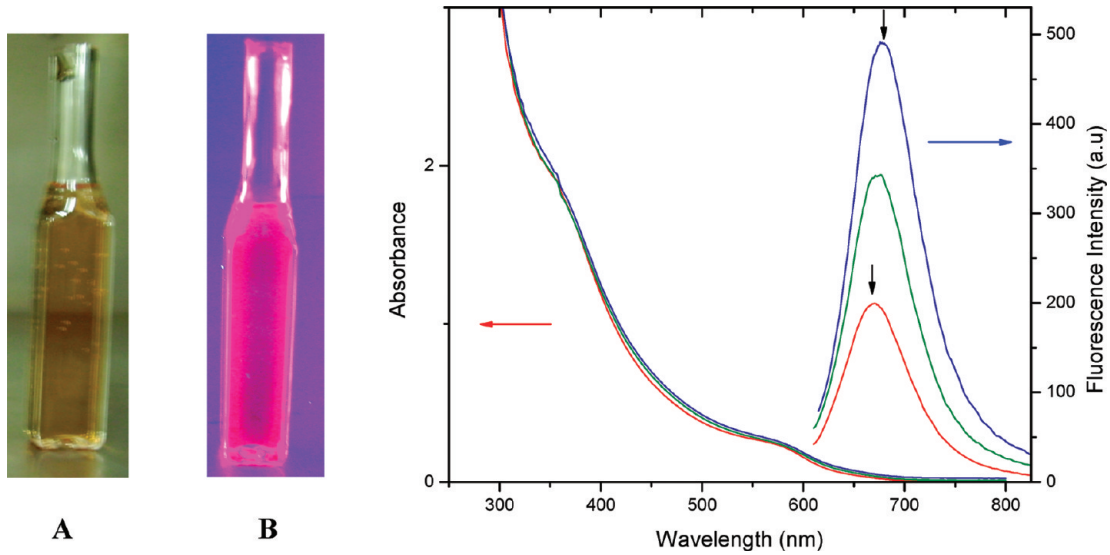

Figure 1. Absorption and fluorescence spectra of fresh and aged Zn/PbS nanocomposites containing $Zn^{2+} = 2 \times 10^{-3}$ mol dm^{-3} for 0.0 days (red line), 20 days (green line), and 40 days (black line) at pH 9.8; $\lambda_{ex} = 620$ nm. Zn/PbS sample in ambient (A) and after ultraviolet illumination (B).

followed by the injection of SH^-, it led to the formation of PbS nanoparticles with a fairly different optical and emission behavior. These nanostructures lacked prominent excitonic band and exhibited a relatively broader emission band with about an order of magnitude smaller quantum efficiency of emission ($\phi < 0.015$).

Aging of the optimized RNA-capped Zn/PbS nanocomposite did not depict any appreciable change in the optical behavior except that the onset of absorption was slightly red-shifted from 1.76 to 1.71 eV. The first 20 days of aging of Zn/PbS particles results in the red shifting of the fluorescence maximum from 669 nm (1.85 eV) to 677 nm (1.82 eV) along with an enhancement of its intensity by more than 1.7-fold. Aging for 40 days enhanced the emission intensity further by about 2.5-fold, and the resulting colloids glowed under UV illumination ($\geq$320 nm) (Figure 1). These colloids exhibit relatively a narrow fluorescence band at 680 nm with fwhm of $\leq$80 nm. It corresponded to the quantum efficiency of fluorescence of 12 $\pm$ 0.2%, which is the highest reported value so far for PbS nanocrystals in the visible range. Aging beyond 40 days, however, resulted in the depletion of fluorescence intensity without any change in the absorption characteristics. Unlike RNA-PbS precursor used in the present work, DNA-mediated PbS exhibit fairly different electronic properties and did not exhibit any emission in the visible region.[13,24]

Electron micrographs of PbS nanoparticles on RNA matrix containing varied amounts of zinc have been presented in Figure 2. PbS nanoparticles with Pb/S molar ratio of 2 are spherical in shape with an average diameter of 6 nm. The addition of 5×10^{-4} mol dm^{-3} of Zn^{2+} to this colloidal PbS solution causes these particles to stick together to form bigger clusters. A further increase in the concentration of Zn^{2+} to 1×10^{-3} mol dm^{-3} results in the formation of chainlike aggregates of different shapes. At higher Zn^{2+} ($\geq 2 \times 10^{-3}$ mol dm^{-3}) these structures start assuming the rodlike nanostructure having a diameter of 25 nm. Aging of these nanocrystals for an initial 20 days induces their unidirectional growth to yield distinct nanowires of about 2 μm length with an aspect ratio of 40, which after aging for 40 days reorganizes to form a superstructure of nanofibers (Figure 2). A change in morphology from nanowires to nanofibers is also supported by anisotropic measurements of the two samples, which demonstrate an increase in anisotropy value from <0.1 to 0.15 upon aging of this colloidal solution (Figure S2 in Supporting Information).

Selected area electron diffraction patterns (SAED) of fresh and aged Zn/PbS particles having a Pb/S molar ratio of 2 consisted of a series of concentric rings indicating them to be polycrystalline in nature (Figure 2d′,f′). Indexing of these patterns in both cases correlates to diffraction peaks (111), (200), (220), and (311), which correspond to the presence of PbS in the face-centered cubic structural form in the composite. Besides, the SAED patterns of aged particles exhibit additional rings depicting reflections at (110), (605), and (222) planes (Figure 2f′) matching to the diffraction pattern of orthorhombic $Zn(OH)_2$.[25]

EDX analysis of FE-SEM images of freshly prepared Zn/PbS colloidal particles deposited on a grid showed the formation of nanoclusters consisting of zinc, lead, and sulfur (not shown). These particles upon aging for 20 days are transformed to nanowires consisting of zinc, lead, and sulfur of almost the same atomic ratios of Pb:Zn:S as observed prior to aging and eventually organize to form bundles of nanowires having lengths of several micrometers and widths of 35−40 nm (Figure 3A). Further aging for about 40 days produced nanofibers of several micrometers in length (Figure S3 in Supporting Information). From various EDX spectra of nanofibers, the chemical composition of the fibrous structure is found to consist of Pb, S, and Zn in the atomic ratios of 2 $\pm$ 0.3 to 1 to 6 $\pm$ 0.4, respectively.

The interaction of different components of RNA with PbS particles and excess ions present in the composite was analyzed by IR and ^{1}H NMR spectroscopy. A comparison of IR spectra of PbS nanocrystals synthesized in the absence and presence of Zn^{2+} reveals that the presence of zinc causes the PO_2^- asymmetric stretching present in sugar moiety to disappear. In addition it depicted a marked shift in the IR peaks to higher energy due to purine and pyrimidine bases in RNA compared to those in its absence (Figure S4 in Supporting Information).

The addition of Zn^{2+} causes the protons due to different purine and pyrimidine bases (H2, H8, and H6), sugar and purine base (H1 and H5′), and sugar moiety (H2′, H3′, H4′, H5′, and H5″) to resonate between 7.5 and 8.4 ppm, 5.5 and 6.2 ppm, and 3.6 and 4.5 ppm, respectively, with a better resolution

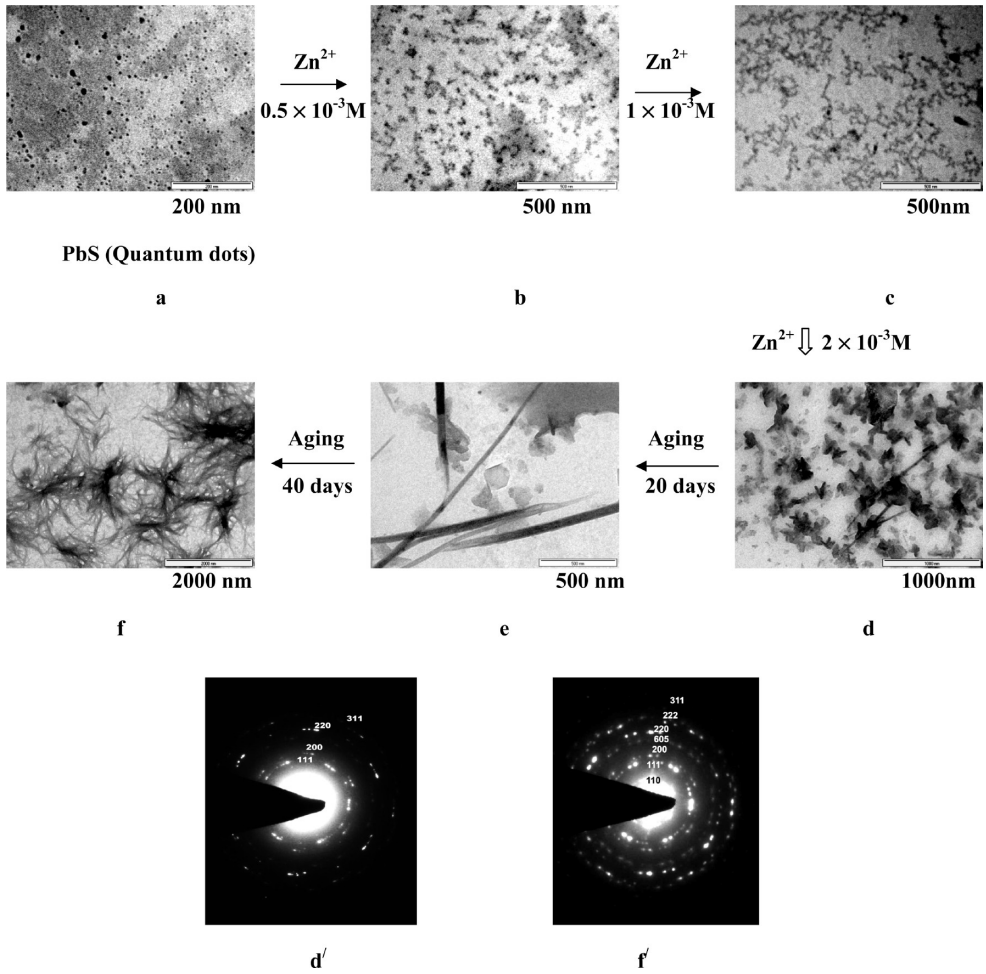

Figure 2. TEM micrographs exhibiting a change in the morphology of PbS particles as a function of added [Zn^{2+}]($\times$ 10^{-3} mol dm^{-3}): 0 (a), 0.5 (b), 1.0 (c), and 2.0 (d) and upon aging them for 20 (e) and 40 days (f). SAED patterns of nanostructures shown in electron micrographs "d" (d′) and "f" (f′).

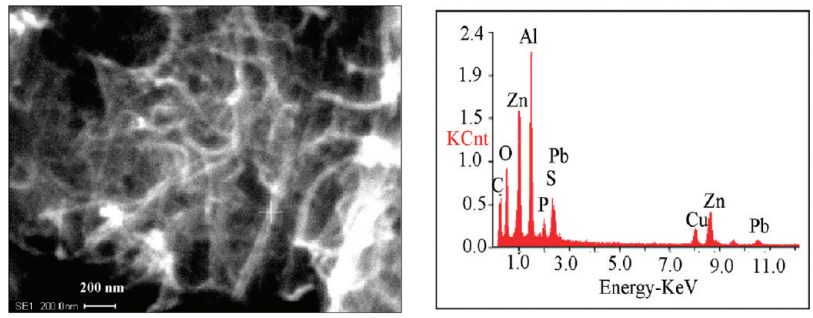

Figure 3. Field emission scanning electron micrograph(s) and EDX analysis of Zn/PbS nanocomposites containing 2 $\times$ 10^{-3} mol dm^{-3} Zn^{2+} and having Pb/S molar ratio of 2 after aging for 20 days.

compared to pure RNA. The peak assigned to the 2′ proton of the hydroxyl group is now split into two peaks (1.8−2.1 ppm) of nearly equal intensities and become more intense. This phenomenon possibly might have arisen because of the reduced exchange of −OH protons due to complexation with Zn/PbS nanocrystals and, consequently, splitting of the hydroxyl proton due to coupling with neighboring C−H proton of the sugar (Figure 4). Thus IR and NMR experiments depict the interaction of Zn^{2+} with phosphate ions, and both of Zn^{2+} and $Pb^{2+}$with −OH of sugar moiety and purine and pyrimidine bases, respectively. The interaction of both Pb^{2+} and Zn^{2+} through 2′ proton of hydroxyl group of the sugar moiety and nucleic bases of RNA may be considered to contribute to the observed difference in electronic properties of RNA-templated PbS and Zn/PbS composites in contrast to that of DNA-mediated PbS[13,24] because of the absence of this functional group in DNA.

The fluorescence due to RNA-templated Zn/PbS nanocomposites in the absence as well as presence of different [Zn^{2+}] decayed in three exponential kinetics having three components lying in nanosecond, tens of nanoseconds, and several tens of nanoseconds time domain (Figure 5). An addition of Zn^{2+} from 0 to 2 $\times$ 10^{-3} mol dm^{-3} to freshly prepared PbS enhanced the average fluorescence lifetime ($\langle\tau\rangle$) of these colloids from 62 to 229 ns (Table 1a). An analysis of the different lifetime

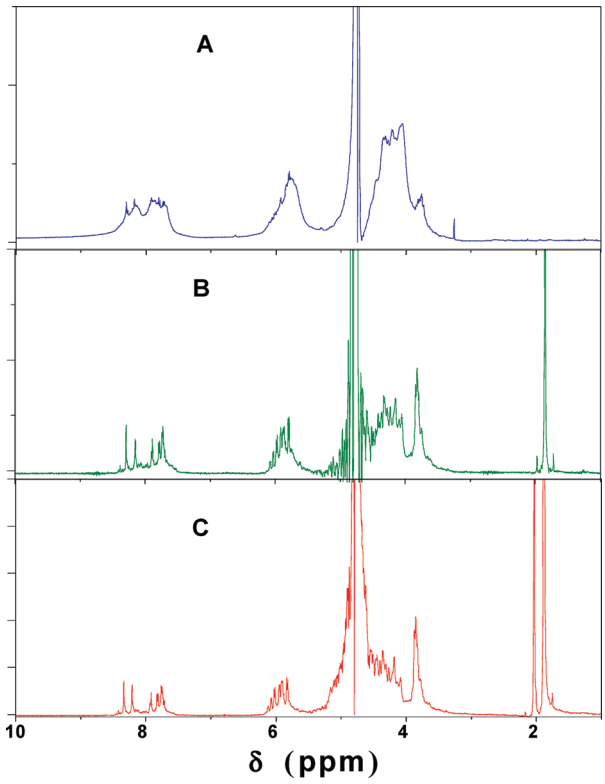

Figure 4. NMR spectra of pure RNA (A), PbS grown on RNA matrix with molar ratio of Pb/S 2 (B), and Zn/PbS grown on RNA matrix containing 2×10^{-3} mol dm^{-3} Zn^{2+} (C).

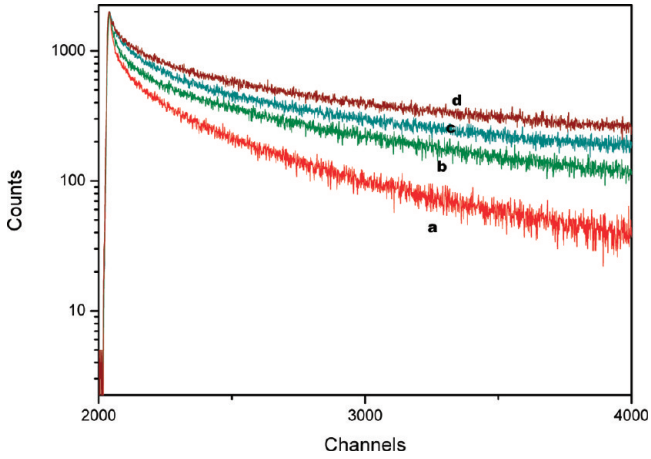

Figure 5. Fluorescence decay curves of Zn/PbS nanocomposites with Pb/S molar ratio of 2 containing different amounts of Zn^{2+} ($\times 10^{-3}$ mol dm^{-3}): 0.0 (a), 1.0 (b), and 2.0 (c) and after aging the particles for 40 days (d). $\lambda_{ex} = 605$ nm. $\lambda_{em} = 675$ nm at pH 9.8. Time calibration $= 1.210196 \times 10^{-10}$ s/channel.

components shows that the lifetime of each of the components is increased more prominently at lower concentration up to 5×10^{-4} mol dm^{-3} and, thereafter, depicted a slight increase up to 2×10^{-3} mol dm^{-3}. On the contrary the lifetime of the third component only is increased significantly upon aging for 40 days from 269 to 308 ns, which enhances $\langle\tau\rangle$ from 229 to 271 ns (Table 1b). An examination of Table 1 reveals that lifetime components corresponding to nanosecond and tens of nanosecond scale have relatively less contribution to the fluorescence yield, i.e., <5 and ≤15%, respectively, compared to the component with longer time constant (≥80%).

A large variation in lifetime of different components from 1.03 to 308 ns indicates the distribution of surface states to varied depths, which though kinetically lie in three distinct ranges (Table 1). From the lifetime data, assuming the activation energy of detrapping as the trap depth and frequency factor of detrapping corresponding to the upper limit of monomolecular reactions, i.e. 10^{13} s^{-1}, the depth of these traps has been estimated to lie between 229 and 370 meV.

The addition of Zn^{2+} ions to PbS with varying molar ratio of Pb/S influenced the electronic properties of PbS in a complex manner. Its addition in stepwise increments to PbS particles having molar ratio of Pb/S = 2 depicts a slight increase in the absorption coefficient in the visible region accompanied with a simultaneous decrease in the UV region with an isosbestic point at 602 nm, which cannot be explained simply by the exchange of Pb^{2+} by Zn^{2+} as ZnS does not have any absorption in the visible region. Moreover the solubility product of ZnS (1.2×10^{-23}) is much larger than PbS (3.4×10^{-28}); therefore, the replacement of Pb^{2+} by Zn^{2+} in PbS is ruled out. It was further verified in a control experiment in which the coating of ZnS on PbS particles[26] results in the formation of nonfluorescing PbS particles, which is contrary to the observations made in the present case.

Morphological changes observed from TEM micrographs (Figure 2) evidently indicate that the presence of Zn^{2+} induces the gradual growth of these particles through several metastable states to eventually form nanofibers upon aging. Remarkably, this change in the morphology from quantum dots to nanofibers is associated with a significant enhancement in the intensity of emission and emission lifetime of charge carriers.

The role of excess Pb^{2+} and Zn^{2+} in the formation of Zn^{2+}/PbS nanocomposite was further analyzed in control experiments designed by adding excess Pb^{2+} to PbS-RNA precursor in the absence of Zn^{2+} and then adding Zn^{2+} to the stoichiometric RNA-mediated PbS. The addition of excess Pb^{2+} (5×10^{-4} mol dm^{-3}) to the precursor colloidal PbS in the absence of Zn^{2+} produces spherical quantum dots with an average particle size of about 5 nm having a size distribution ranging from 2 to 16 nm (Figure S5 in Supporting Information). Aging of these particles did not exhibit any morphological changes as observed in the presence of Zn^{2+} ions and get coagulated within 10 days. Moreover, an enhancement in the intensity of emission due to these particles was only about 1.8 times to those of freshly prepared PbS particles, which corresponded to a quantum efficiency of about 0.012. The addition of excess Zn^{2+} to the stoichiometric colloidal PbS−RNA solution also did not demonstrate any morphological changes for both fresh as well as aged particles. Interestingly, the stoichiometric colloidal PbS−RNA particles themselves were nonemissive, but in the presence of Zn^{2+} their quantum efficiency is enhanced to 0.011, which is though about an order of magnitude less to that observed with the presently used precursor PbS−RNA sample.

The added zinc may bind to various sites on RNA,[27] which is also evidenced in the present work by its interaction with PO_2^-, −OH of sugar, purine, and pyrimidine bases of RNA matrix of Zn/PbS particles (Figure 4 and Figure S4 in Supporting Information). EDX analysis of an FE-SEM image of aged Zn/PbS colloids indicates the presence of more of Zn^{2+} in nanofibers bound to RNA (Figure S3 in Supporting Information). Considering relatively higher concentrations of Zn^{2+} and taking into account the pK_a of 9.6 for Zn^{2+} hydrate,[28] one would expect these ions to be present largely (~60%) as zinc hydroxides at a pH of 9.8. Indeed the formation of orthorhombic $Zn(OH)_2$ is revealed by the indexing of SAED patterns of the aged particles (Figure 2f′).

TABLE 1: Effect of [Zn^{2+}] on the Emission Lifetime of Q-PbS. (λ_{ex} = 605 nm; λ_{em} = 680 nm)[a]

(a) Fresh Samples

[Zn^{2+}] ($\times 10^{-4}$ mol dm^{-3})	lifetime (ns) component 1 τ_1	component 1 emission %	component 2 τ_2	component 2 emission %	component 3 τ_3	component 3 emission %	$\langle\tau\rangle$ (ns)	χ^2
0	1.03 (0.22)	7.61	12.8 (0.048)	20.97	82.5 (0.025)	71.42	62	1.1
1	2.20 (0.07)	3.92	25.5 (0.02)	15.75	185.0 (0.017)	80.34	152	1.1
5	3.36 (0.05)	3.52	26.4 (0.03)	13.68	251.0 (0.017)	82.80	211	1.1
10	3.39 (0.05)	3.16	27.6 (0.03)	14.39	257.0 (0.018)	82.46	216	1.0
15	3.44 (0.05)	3.19	28.2 (0.03)	14.48	261.0 (0.018)	82.33	219	1.0
20	3.50 (0.05)	2.51	28.3 (0.03)	14.20	269.0 (0.198)	83.29	229	1.1

(b) Effect of Aging on the Emission Lifetime of Q-PbS

time (days)	lifetime (ns) component 1 τ_1	component 1 emission %	component 2 τ_2	component 2 emission %	component 3 τ_3	component 3 emission %	$\langle\tau\rangle$ (ns)	χ^2
0	3.50 (0.05)	2.51	28.3 (0.03)	14.20	269 (0.198)	83.29	229	1.1
20	2.88 (0.05)	1.67	30.7 (0.03)	12.15	304 (0.022)	86.18	266	1.1
40	2.98 (0.05)	1.64	31.0 (0.03)	11.41	308 (0.024)	86.96	271	1.1

[a] Values in parentheses are pre-exponential factors corresponding to respective τ.

Both Pb^{2+} and Zn^{2+} have very similar binding affinities for different functional sites of RNA[27] except that Pb^{2+} does not show any interaction with PO_2^-. But the observation of a relatively less prominent excitonic absorption band associated with a drastic reduction in the fluorescence yield for Zn/PbS colloids obtained by simply reversing the order of addition of Pb^{2+} and Zn^{2+}, suggest a difference in their nature of interaction with different sites of RNA matrix on the surface of nanoparticle. In fact in the reversed addition, Zn^{2+} having about seven times higher concentration to that of Pb^{2+}, might occupy most of the functional sites of RNA, which may not be fully replaced by the addition of relatively lower [Pb^{2+}] afterward. It evidently indicates that Pb^{2+} and Zn^{2+} passivates the surface of Zn/PbS nanostructure differently. Since Pb^{2+} does not bind to PO_2^-, it may be concluded that the prior binding of Zn^{2+} through −OH of sugar and other bases favorably enhance the fluorescence yield. Further, in the absence of any evidence for the formation of ZnS and also the observation that the coating of ZnS on PbS[26] does not contribute to the enhancement of fluorescence yield, it may be argued that the addition of excess Zn^{2+} is likely to substitute free Pb^{2+} in the Zn/PbS nanostructure. At a pH of 9.8, Zn^{2+} will largely be present as $Zn(OH)_2$, which might surround the small band gap PbS to enhance its quantum efficiency of emission. A very similar effect of the addition of excess Zn^{2+} has been observed earlier for DNA-mediated colloidal Q-CdS upon modifying its surface by growing ZnS phase.[29]

A drastic change in emission wavelength for RNA-capped PbS/Zn/PbS colloids compared to DNA-capped PbS might have arisen because of the difference in the passivation of the surface of particles in the two cases and, thereby, manipulating the density of surface traps involved in radiative and nonradiative transition. In the former case it possibly creates more of relatively shallower traps inducing radiative recombination corresponding to 680 nm emission unlike to DNA-capped PbS.[24] The latter system did not exhibit any detectable emission in this wavelength range at room temperature, and this observation has been understood by considering the relaxation of the photoexcited species to be primarily nonradiative.

The excess zinc and lead might also remove the additional RNA moiety attached to the outer shell of Q-PbS particles. A systematic removal of the protective shell of RNA from these nanoclusters possibly causes them to reorganize upon aging and results in their growth in one direction to yield chainlike aggregates and to eventually form nanowires (Figure 3). On the basis of spectroscopic measurements and analysis of the chemical composition of nanofibers arrived from EDX measurements, their structure can be conceived containing two Zn^{2+}−RNA, Zn^{2+}/Pb^{2+}−RNA species attached to Zn^{2+}/PbS−RNA nanocomposite (Scheme 1, structure B) in which Zn^{2+} centers would largely be present as $Zn(OH)_2$. Nanofibers may thus be formed by linking of rodlike nanostructures through Zn^{2+} upon aging for over a period of about 40 days. The self-organization of these nanoparticles to nanofibers associated with an increase in crystallinity and enhancement of fluorescence can be explained due to the strong dipole−dipole interparticle interaction upon the removal of the protective shell of RNA similar to that interpreted earlier by Tang et al.[30] for the transformation of thioglycolic acid stabilized CdTe nanoparticles into luminescent nanowires.

In other control experiments none of the components of RNA, namely, nucleosides (A, C, G, and U) and nucleotides (AMP, GMP, CMP, and UMP),[31] were found to stabilize the precursor PbS particles. Obviously, it is the flexibility of three-dimensional structure of RNA owing to its characteristic folding in the presence of excess Zn^{2+} and Pb^{2+}, which appears to be necessary for the stabilization and formation of different nanostructures.

The excess Zn^{2+} binds to the surface of these particles through RNA influencing the shallow as well as deep traps responsible for nonradiative transition as indicated by the respective decrease and increase in percent emission corresponding to short and long time constant components in lifetime data (Table 1). Similarly, increased fluorescence quantum efficiency is also supported by fluorescence lifetime measurements in which a significant increase in the fluorescence lifetime corresponding to the longer time constant is observed. Such a correlation in the steady-state fluorescence changes and lifetime measurements is in accordance to the classical theory of fluorescence.[32] A change in morphology of these nanostructures from spherical quantum dots to nanofibers with high aspect ratio occurring via the formation of nanowires might also contribute to the enhancement in fluorescence lifetime and quantum efficiency

SCHEME 1: Structure Depicting Interaction of Zn^{2+} with RNA (A) and Structure of Aged Zn/PbS Nanostructure on RNA Matrix with High Zinc Concentration (B)

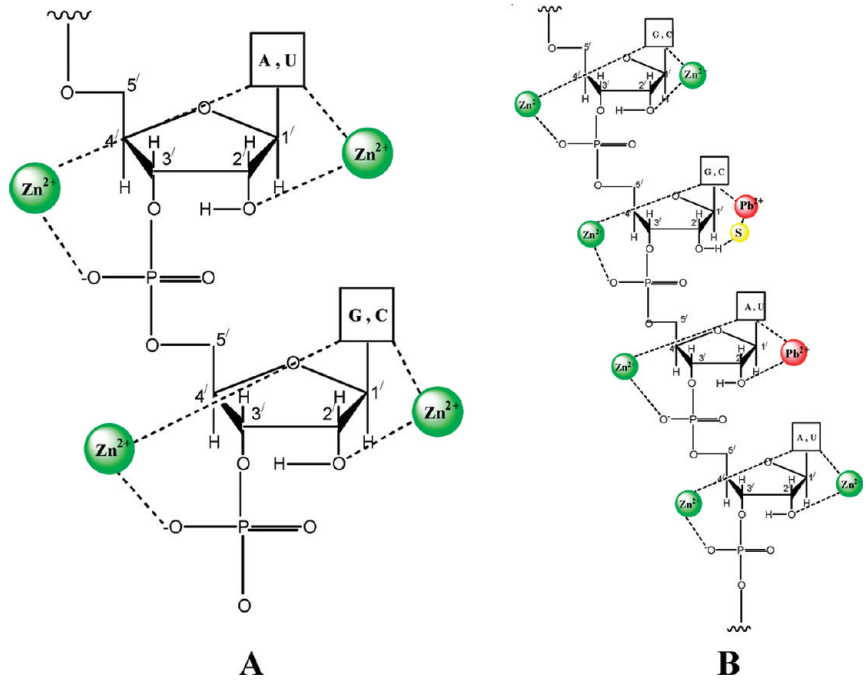

of emission due to increased surface area and crystallinity compared to those of quantum dots. The two-dimensional quantum confinement of charge carriers along the nanofiber/nanowire is expected to cause an increase in the density of surface traps resulting in the increased oscillator strength. The trapped charge carriers possibly undergo increased radiative recombination and would thereby enhance the fluorescence lifetime and the quantum efficiency of emission. Evidently, the prior addition of Pb^{2+} followed by Zn^{2+} in the used molar ratio bring the observed changes in electronic properties and are required for the growth of the fluorescing supernanostructure as shown in Scheme 1 (structure B).

Conclusions

In summary this paper describes a novel methodology to control the architecture of PbS-based nanostructures. Synthesis of PbS in biopolymeric matrix and thereafter making its composite by adding Zn^{2+} ions produces fluorescent PbS with high quantum efficiency in the visible region. Interestingly, a variation in the composition of Zn^{2+} generates supramolecular assemblies of varied morphology consisting of Zn^{2+}/PbS nanocomposites. The possibility of effective sensitization of these supernanostructures by light of wavelength >600 nm is a remarkable achievement as regards to their utilization for solar applications.[1,18] Multifunctionality of RNA contributes to the observed electronic properties in a cooperative manner. The electronic and structural features of these material(s) make them the promising candidate for applications in fabrication of nanoscale photonic devices and visible detector technology.

Experimental Section

Materials. Lead acetate was obtained from Qualigens, adenine (A), guanine (G), cytosine (C), uracil (U), adenosine monophosphate (AMP), guanosine monophosphate (GMP), cytosine monophosphate (CMP), and uracil monophosphate (UMP) were obtained from Sigma, ribonucleic acid derived from yeast having phosphorus contents 8% and nitrogen 15% (RNA), Product code 184911, was from SRL, nile blue and anhydrous zinc acetate were from Fluka, sodium hydroxide was from BDH, and nitrogen gas and oxygen gas (Grade 1, purity >99.99%) were from Sigma. All chemicals used were of analytical grade and were used as received.

The used RNA sample is a heterogeneous mixture of RNA molecules with varied molecular weights.

Equipment. Electronic spectra were recorded on a Shimadzu UV2100S spectrophotometer. Emission measurements were made on a Shimadzu RF-5301PC spectrofluorophotometer. Electron micrographs and selected area electron diffraction were measured on a Fei-Philips Morgagni 268D Digital TEM and FEI-TECNAI 200 kv Digital TEM with an image analysis system having variable magnifications up to 280000× 1100000×, respectively. Surface morphologies and quantitative analysis of synthesized nanoparticles were performed on QUANTA 200-FEG Digital SEM with EDX facility equipped with a CCD camera. The ^1H NMR spectra were recorded on a Bruker Avance 500 (500 MHz) spectrometer in H_2O. IR spectra were measured on a Thermonicolet Nexus FTIR spectrophotometer. The fluorescence lifetime in nanosecond time domain was recorded on a Horiba Jobin Yvon "FluoroCube Fluorescence Lifetime System" equipped with NanoLEDs and LDs. With these systems the emitted photons were detected by using a Hamamatsu (R 3809 U) photomultiplier and a thermoelectrically cooled TBX-04-D detector.

The quantum efficiency of fluorescence in steady-state experiments was determined by using a relative method employing an optically matched solution of nile blue dye as reference.[33]

Indexing of electron diffraction pattern corresponding to different rings was carried out by using a ratio method. Miller indices were then assigned by correlating the reflections with the respective expected known structure(s). Besides, these rings were also matched with their respective authentic samples/literature data.

Synthesis of RNA Capped Zn/PbS (PbS + Zn^{2+}) Nanocomposites. RNA-mediated PbS nanoparticles were synthesized as described earlier[15] by the addition of SH^- (1.5×10^{-4} mol dm^{-3}) to the deaerated Pb^{2+} solution (3×10^{-4} mol dm^{-3}) containing 0.016 g/100 mL of RNA at 4 °C and pH of 9.8. RNA-capped Zn/PbS (PbS + Zn^{2+}) nanocomposites were then synthesized by the gradual addition of varied amounts of zinc acetate (1×10^{-4} to 2×10^{-3} mol dm^{-3}) to the above-prepared deaerated colloidal solution of RNA-mediated PbS nanoparticles at 4 °C. The pH of the solutions was maintained at 9.8 at each step of synthesis.

Acknowledgment. The financial support of DST, New Delhi is gratefully acknowledged to undertake this work. A.J. is thankful to CSIR, New Delhi for the award of SRF. Thanks are also due to the Director, AIIMS, New Delhi and Prof. & Head, IIC, IITR, Roorkee for providing us the facilities of TEM and AFM, FE-SEM, and Single Photon Counter, respectively, and to Mr. Vinit Kumar for help in the analysis of one of the SAED patterns.

Supporting Information Available: More information on characterization of these nanostructures by absorption, emission, anisotropy, FESEM, IR, and TEM. This material is available free of charge via the Internet at http://pubs.acs.org.

References and Notes

(1) Fick, J.; Martucci, A. *Encyclopedia of Nanoscience and Nanotechnology*; Nalwa, H. S., Ed.; American Scientific Publishers: Stevenson Ranch, CA, 2004; Vol. 4, pp 481−504.

(2) Sargent, E. H. Infrared Quantum Dots. *Adv. Mater.* **2005**, *17*, 515–523.

(3) Hines, M. A.; Scholes, G. D. Colloidal PbS Nanocrystals with Size-Tunable Near-Infrared Emission: Observation of Post-Synthesis Self-Narrowing of the Particle Size Distribution. *Adv. Mater.* **2003**, *15*, 1844–1849.

(4) Yang, Y.; Nogami, M.; Shi, J.; Chen, H.; Liu, Y.; Qian, S. Self-Assembled Semiconductor Capped Metal Composite Nanoparticles Embedded in $BaTiO_3$ Thin Films for Nonlinear Optical Applications. *J. Mater. Chem.* **2003**, *13*, 3026–3032.

(5) Lu, S. W.; Sohling, U.; Menning, M.; Schmidt, H. Nonlinear Optical Properties of Lead Sulfide Nanocrystals in Polymeric Coatings. *Nanotechnology* **2002**, *13*, 669–673.

(6) Rogach, A. L.; Eychmüller, A.; Hickey, S. G.; Kershaw, S. V. Infrared Emitting Colloidal Nanocrystals: Synthesis, Assembly, Spectroscopy and Applications. *Small* **2007**, *3*, 536–557.

(7) Niemeyer, C. M. Nanoparticles, Proteins, and Nucleic Acids: Biotechnology Meets Materials Science. *Angew. Chem., Int. Ed.* **2001**, *40*, 4128–4158.

(8) Schmid, G. *Nanoparticles*; Wiley-VCH Verlag GmbH and Co. KGaA, Weinheim Press: Germany, 2004.

(9) Srivastava, S.; Verma, A.; Frankamp, B. L.; Rotello, V. M. Controlled Assembly of Protein Nanoparticle Composites through Protein Surface Recognition. *Adv. Mater.* **2005**, *17*, 617–621.

(10) Bigham, S. R.; Coffer, J. L. The Influence of Adenine Content on the Properties of Q-CdS Clusters Stabilized by Polynucleotides. *Colloids Surf., A* **1995**, *95*, 211–219.

(11) Li, X.; Coffer, J. L. Effect of Pressure on the Photoluminescence of Polynucleotide-Stabilized Cadmium Sulfide Nanocrystals. *Chem. Mater.* **1999**, *11*, 2326–2330.

(12) Bigham, S. R.; Coffer, J. L. Themochemical Passivation of DNA-Stabilized Q-Cadmium Sulfide Naoparticles. *J. Cluster Sci.* **2000**, *11*, 359–372.

(13) Levina, L.; Sukhovatkin, V.; Musikhin, S.; Cauchi, S.; Nisman, R.; Bazzet-Jones, D. P.; Sargent, E. H. Efficient Infrared-Emitting PbS Quantum Dots Grown on DNA and Stable in Aqueous Solution and Blood Plasma. *Adv. Mater.* **2005**, *17*, 1854–1857.

(14) Alivisatos, A. P.; Johnsson, K. P.; Peng, X.; Wilson, T. E.; Loweth, C. J.; Bruchez, M. P.; Schultz, P. G. Organization of Nanocrystal Molecules Using DNA. *Nature* **1996**, *382*, 609–611.

(15) Kumar, A.; Jakhmola, A. RNA-Mediated Fluorescent Q-PbS Nanoparticles. *Langmuir* **2007**, *23*, 2915–2918.

(16) Feldheim, D. L.; Eaton, B. E. Selection of Biomolecules Capable of Mediating the Formation of Nanocrystals. *ACS Nano* **2007**, *1*, 154–159.

(17) Ma, N.; Dooley, C. J.; Kelley, S. O. RNA-Templated Semiconductor Nanocrystals. *J. Am. Chem. Soc.* **2006**, *128*, 12598–12599.

(18) Mcdonald, S. A.; Konstantatos, G.; Zhang, S.; Cyri, P. W.; Kelm, E. J. D.; Levina, L.; Sargent, E. H. Solution-**P**rocessed PbS Quantum Dot Infrared Photodetectors and Photovoltaics. *Nat. Mater.* **2005**, *4*, 138–142.

(19) Plass, R.; Pelet, S.; Krueger, J.; Grätzel, M.; Bach, U. Quantum Dot Sensitization of Organic-Inorganic Hybrid Solar Cells. *J. Phys. Chem. B* **2002**, *106*, 7578–7580.

(20) Wise, F. W. Lead-salt Quantum Dots: The Limit of Strong Quantum Confinement. *Acc. Chem. Res.* **2000**, *33*, 773–780.

(21) Alivisatos, A. P. The Use of Nanocrystals in Biological Detection. *Nat. Biotechnol.* **2004**, *22*, 47–52.

(22) Michalet, X.; Pinaud, F.; Lacoste, T. D.; Dahan, M.; Bruchez, M. P.; Alivisatos, A. P.; Weiss, S. Properties of Fluorescent Semiconductor Nanocrystals and Their Application in Biological Labeling. *Single Mol.* **2001**, *4*, 261–276.

(23) Nelson, D. L.; Cox, M. M. *Lehninger Principles of Biochemistry*, 4th ed.; Freeman W. H. and Co.: New York, 2004; pp 277−291.

(24) Patel, A. A.; Wu, F.; Zhang, J. Z.; Martinez, C. L. T.; Mehra, R. K.; Yang, Y.; Risbud, S. H. Synthesis, Optical Spectroscopy and Ultrafast Electron Dynamics of PbS Nanoparticles with Different Surface Capping. *J. Phys. Chem. B* **2000**, *104*, 11598–11605.

(25) Joint Committee on Powder Diffraction Standards. *Inorganic Index to the Powder Diffraction File*; International Center of Diffraction Data: Newtown Square, PA,1971; pp 380, 627, 638, 641, 645, 683.

(26) In a control experiment ZnS-coated PbS particles were prepared by adding excess Zn^{2+} (1.5×10^{-4} mol dm^{-3}) to RNA capped PbS particles followed by the injection of the stoichiometric amount of SH^-.

(27) Ennifar, E.; Walter, P.; Dumas, P. A Crystallographic Study of the Binding of 13 Metal Ions to Two Related RNA Duplexes. *Nucleic Acids Res.* **2003**, *31*, 2671–2682.

(28) Ciesiolka, J.; Michalowski, D.; Wrzesinski, J.; Krajewski, J.; Krzyzosiak, W. J. Patterns of Cleavages Induced by Lead Ions in Defined RNA Secondary Structure Motifs. *J. Mol. Biol.* **1998**, *275*, 211–220.

(29) Bigham, S. R.; Coffer, J. L. Deactivation of Q-CdS Photoluminescence through Polynucleotide Surface Binding. *J. Phys. Chem.* **1992**, *96*, 10581–10584.

(30) Tang, Z.; Kotov, N. A.; Giersig, M. Spontaneous Organization of Single CdTe Nanoparticles into Luminescent Nanowires. *Science* **2002**, *297*, 237–240.

(31) In control experiments it is observed that neither of nucleosides (A, G, C, and U) and nucleotides (AMP, GMP, CMP, UMP) (0.016 g/100 mL each) nor their equimolar mixtures (0.004 g/100 mL each) were effective in stabilizing the precursor PbS particles under similar experimental conditions as employed in the present work. It resulted in the formation of dull brown solutions, which precipitated within a few minutes.

(32) Lakowicz, J. R. *Principles of Fluorescence Spectroscopy*; Kluwer Academic Publishers/Plenum Press: New York, 1999; pp 14−15.

(33) Sens, R.; Drexhage, K. H. Fluorescence Quantum Yield of Oxazine and Carbazine Laser Dyes. *J. Lumin.* **1981**, *24/25*, 709–712.

JP811402H